DEUTSCHES ELEKTRONEN-SYNCHROTRON DESY

DESY SR-83-10
August 1983

ELECTRONIC BAND STRUCTURE OF SOLID CO_2 AS DETERMINED FROM THE hν-DEPENDENCE OF PHOTOELECTRON EMISSION

by

J.-H. Fock and H.-J. Lau

II. Institut für Experimentalphysik, Universität Hamburg

E.E. Koch

Hamburger Synchrotronstrahlungslabor HASYLAB at DESY

ISSN 0723-7979

NOTKESTRASSE 85 · 2 HAMBURG 52

To be sure that your preprints are promptly included in the
HIGH ENERGY PHYSICS INDEX ,
send them to the following address (if possible by air mail) :

DESY
Bibliothek
Notkestrasse 85
2 Hamburg 52
Germany

Electronic band structure of solid CO_2 as determined from the hν-dependence of photoelectron emission*

J.-H. Fock and H.-J. Lau
II. Institut für Experimentalphysik, Universität Hamburg
D-2000 Hamburg 50, Federal Republic of Germany
and
E.E. Koch
Hamburger Synchrotronstrahlungslabor HASYLAB at DESY
D-2000 Hamburg 52, Federal Republic of Germany

Abstract

Photoelectron energy distribution curves from solid CO_2 have been determined for excitation energies from hν = 14 up to 40 eV using synchrotron radiation. A 1:1 correspondence to the gas phase photoelectron spectrum is observed for the occupied molecular orbitals. The vertical binding energies E_B^V (E_{VAC} = 0) and widths (fwhm) of the valence bands of solid CO_2 are determined to be 13.0 eV and 0.95 eV ($1\pi_g$); 16.7 eV and 1.1 eV ($1\pi_u$); 17.6 eV and 0.85 eV ($3\sigma_u$) and 18.8 eV and 0.8 eV ($4\sigma_g$) for the individual bands respectively. The partial photoemission cross sections differ importantly from those of the gas phase in exhibiting pronounced maxima at 5.3 eV ($1\pi_g$), 4.4 - 5.5 eV ($1\pi_u + 3\sigma_u$) and 4.2 eV ($4\sigma_g$) above the vacuum level, which is attributed to effects of high density of final (conduction band) states. Further weaker maxima are observed at higher photon energies. Contrary to the case for the gas phase, the resonances are unperturbed in the solid by degenerate autoionizing molecular Rydberg states. The molecular origin of the resonances in the continuum is discussed and related to x-ray absorption spectra, electron scattering data and to theoretical cross-section calculations. It is shown that the same set of resonances is observed in the different experiments. The resonances occur however at different energies due to different Coulomb interaction. The photoemission results presented provide also a key to the hitherto unexplained optical spectrum of solid CO_2 in the VUV range, making possible an assignment of the structures observed to Frenkel-type excitons ($h\nu \lesssim 15$ eV) and interband transitions ($h\nu \gtrsim 15$ eV).

*Submitted to Chemical Physics

Work supported in part by Bundesministerium für Forschung und Technologie (BMFT) from Funds for Research with Synchrotron Radiation

ISSN 0723-7979

1. Introduction

Recently we have reported on the striking observation of pronounced resonances in the partial cross sections in the valence band photoemission from solid nitrogen, resonances which are located just above threshold, (i.e., at roughly 3.0 eV above the vacuum level) (1). In contrast to the case of gas phase photoemission, these strong resonances were found to be unperturbed by degenerate autoionizing molecular Rydberg states and have been interpreted in a solid state band structure picture as due to high density of conduction band final states. In the case of solid N_2 we discussed the molecular origin of these final states and related them to the π_g negative-ion shape resonance.

In the course of a systematic study of the band structure of condensed simple di- and tri-atomic gases we have chosen solid CO_2 for more intense study because of its role as the prototypical molecular crystal composed of triatomic molecules. The photoelectron spectrum of gaseous CO_2 has been the subject of several experimental (2-4) and theoretical (5-7) investigations, and the binding energies and symmetries of the occupied molecular orbitals (MO's) are well established. Also the photoelectron branching ratios and partial photoionisation cross sections (8-11) as well as the β-parameters (12-14) have recently been determined and discussed in comparison with theoretical studies (12,15-21). For solid CO_2 there is, however, little information available. Only a not well resolved HeII spectrum for solid CO_2 has recently been reported, (22) and even the pronounced sharp features observed in the VUV-optical spectrum (23) in the range 10 eV $\leq h\nu \leq$ 15 eV have not yet been assigned.

In the present paper we report on the measurement for an extended range of energies of the exciting photons of photoelectron energy distribution curves (EDC's) from solid CO_2. In addition to determining the binding energies and widths of the bands derived from the outer filled molecular orbitals (MO's), we

obtained the partial photoionization cross-sections for the initial states as a function of excitation energy, thereby gaining important information concerning the higher conduction band states. For solid CO_2 as for solid N_2 earlier, a major result of our investigation has been the observation of pronounced maxima in the continuum 4.2 - 5.3 eV above the threshold for each of the partial cross sections. On the basis of our experimental findings and by comparison to x-ray absorption spectra electron scattering data and cross section calculations we discuss the molecular parentage of the electronic band structure and optical spectra. It appears now that cross section determinations close to threshold for solid di- and triatomic molecules are generally not hampered by degenerate autoionizing Rydberg states which make such measurements and their interpretation difficult or even impossible in the gas phase. Thus we suggest that photoemission intensity measurements from molecular crystals may be more useful in testing calculations and various theoretical models for final state effects. At the same time our experiments show the importance of effects characteristic for the solid state such as band formation and intermolecular charge transfer excitations. The careful comparison of gas-phase and solid-phase spectra and of data from different spectroscopies such as x-ray absorption, photoemission and electron scattering, yields valuable insight into the nature of the final states and their molecular parentage. It can be shown that the same set of resonances is observed in the different kinds of experiments. These resonances are spread over the discrete and continuous part of the spectrum, merely shifted in energy according to the different strength of Coulomb interacting, namely electron-core hole, electron-valence hole and electron-neutral molecule respectively.

Finally we can use the results of our photoemission study to interprete the hitherto unassigned structure in the VUV-spectrum of solid CO_2 (23). In this way we also obtain some insight into the problem of making assignments for the CO_2 gas phase absorption spectrum, a long-standing problem in VUV-absorption spectroscopy (see e.g. ref. (7)).

2. Experimental Details

We used for our measurements the previously described (24) 3 m normal incidence monochromator at the HASYLAB laboratory in Hamburg which receives synchrotron radiation from the DORIS II electron-positron storage ring. Light from the monochromator is focused onto the sample located in the center of an ultra high vacuum (UHV) experimental chamber. The base pressure is 5×10^{-10} mbar. The chamber is equipped with a He flowcryostat, a gas handling and inlet system and an angle integrating, double-pass, cylindrical-mirror analyzer (CMA) (25,26). The details of the set-up are shown in Fig. 1. Photon energies ranged from 10 eV to 40 eV with 0.3 nm resolution (corresponding to ~ 0.1 eV at 20 eV) in the whole range. The CMA was operated in the retarding mode in order to obtain a constant resolution ΔE. We chose $\Delta E = 0.20$ eV for $h\nu \leq 30$ eV and $\Delta E = 0.65$ eV for $h\nu \geq 25$ eV. Thus the overall resolution (monochromator and electron energy analyzer) was basically determined by the electron analyzer. It was in all cases sufficient for an accurate determination of EDC-features which were found to have widths ranging between 0.8 eV and 1.1 eV (fwhm). EDC's measured in the region of overlapping $h\nu$ were used for normalizing spectra taken with different ΔE with respect to each other.

For a determination of photoemission intensities in the retarding mode of the CMA with a constant pass energy E_{pass} one must observe that the source volume, from which electrons are accepted, changes with the kinetic energy E_{kin} of the photoelectrons; that is, the emitting area F changes according to (25,26)

$$F = F_o \left(\frac{E_{pass}}{E_{kin}}\right) \quad ,$$

where F_o is the circular aperture of the analyzer. In our case F_o has a diameter of d = 4 mm. The illuminated spot on the sample, however, was only about 1 mm in diameter. This assured that, for the parameters used in our experiment, the analyzer source volume was always much larger than the illuminated spot on the sample from where electrons were emitted. Therefore we

can assume that the transmission of the analyzer was constant, independent of E_{kin}. Only for very low kinetic energies might this assumption be in error, since grid scattering and possible residual magnetic fields around the sample and within the interior of the analyzer could reduce the transmission. Such effects would lead to an underestimation of intensities in the spectra at low E_{kin}. In any case our experience of comparing EDC's from different samples persuades us that no distinct structures or peaks are introduced in the spectra as a result of an unknown exact transmission function.

The geometry used for the experiments is depicted in Fig. 1. The light propagation vector, sample normal and axis of the electron analyzer are coplanar. The CMA accepts electrons in a cone between 36.3° and 48.3° with respect to its axis. Thus with polycrystalline samples the set-up can be characterized as having angle-integrating geometry free from angular effects.

High purity (99.998 %) CO_2 gas was condensed under UHV conditions (pressure before and after condensation 5 x 10^{-10} Torr) from a capillary on a Helium-cooled gold substrate (Fig. 1). The temperature of the substrate was ~ 20 K. Under these conditions CO_2 forms polycrystalline films of cubic Pa3 symmetry (27). To avoid charging of the samples, which can be a serious source of error in photoemission from insulators, the sample thickness of the CO_2 films was limited to roughly 10 nm. Also, the samples were changed and fresh samples were prepared as soon as any sign of charging was noticable during extended periods of data taking. In this way we were able to limit errors in peak positions to a value $\lesssim$ 0.15 eV. The reproducibility from sample to sample of measurements of intensities at the peak was roughly 10 %.

For the determination of photoemission intensities, the EDC's for each excitation energy were normalized to the intensity of the photon flux impinging on the sample. Secondly, a smooth structureless background was subtracted from direct emission

peaks to account for electrons originating from the aged gold substrate and for scattered secondary electrons. Finally, the area under each primary emission peak in the EDC's was determined by fitting the experimentally determined three peak structure by four gaussians corresponding to the four uppermost MO's (see Fig. 3). It turned out that for all photon energies a fit with one gaussian for each MO was sufficient.

As we discussed above, the largest uncertainity in the cross section determination rests in the unknown transmission function of the electron analyzer. It contributes most of the total errors in the relative cross sections which we estimate may be as high as 30 %.

3. Results and Discussion

3a Assignments, valence band binding energies and relaxation

In Fig. 2 is shown a family of EDC's for solid CO_2 at different photon energies. The three main features for direct emission from solid CO_2 are clearly visible. While the uppermost band with highest kinetic energy is well separated from the rest, several other bands coalesce to form a double peaked structure at lower kinetic energies. The direct emission features are decomposed into four partly overlapping bands as indicated in Fig. 3 for one particular photon energy. Thus a clear one-to-one correspondence to the gas phase photoelectron spectrum of CO_2 (4,5) emerges, (Fig. 3) and it is easy to assign the peaks for solid CO_2 to the photoemission from valence bands formed by the $1\pi_g$, $1\pi_u$, $3\sigma_u$ and $4\sigma_g$ MO's of the CO_2 molecule respectively. The resulting vertical binding energies E_B^v are 13.0 ; 16.7 ; 17.6 and 18.8 eV, respectively, with reference to the vacuum level (E_{VAC} = 0) of the sample.

These energies, as well as adiabatic binding energies E_B^{ad} are compiled in Table 1. Adiabatic binding energies were determined by fitting the experimental EDC's with gaussians and by using

$E_B^{ad} = E_B^v - 1.2\ \Gamma$, where Γ is the half width (FWHM) for each band. Gas phase values are also given in Table 1 for comparison.

From these data we obtain a rigid gas-to-solid shift (relaxation energy) towards lower binding energies of $E_R^v = 0.7 \pm 0.2$ eV for all four emission bands. The reduced ionization potentials in monomolecular crystals as compared to the gas phase photoemission of the constituent molecule are caused by initial state shifts and final state shifts which cannot be determined separately in a photoemission experiment. Possible origins to these shifts have been considered previously and several mechanisms have been suggested (see e.g. ref. 28,29): Firstly, a binding energy shift may occur, which effects the initial state of individual orbitals taking part in chemical bonding and leads to the observation of differential shifts of molecular orbitals. For adsorbed layers of molecules on metal surfaces this is a common situation. In bulk molecular crystals, however, shifts due to chemical bonding are generally not observed.

Secondly, the chemical shift or cage effect can alter initial states because of a changed chemical environment. Thirdly, the relaxation shift may simply be caused by screening of the positive hole left behind in the photoemission process and is thus a final state effect. This relaxation mechanism for solid molecular gases has previously been discussed within the framework of the Mott-Littleton model (30-32). A hole polarization energy of $P_t = 1.2$ eV was estimated for solid CO_2 within a simple macroscopic continuum model as the energy difference between the screened hole and the free ion (32). This value lies between the observed adiabatic and vertical ionization potential shifts (Table 1) and has to be considered as the main contribution to the total observed shift. However, an additional smaller contribution from a chemical shift cannot be ruled out. A binding energy shift can be excluded, since we do not observe significant differential shifts of individual orbitals.

Apart from the shift in bonding energy the widths of the photoemission bands are of considerable interest. For all four valence MO's we observe a considerable broadening up to ~ 1.1 eV in the solid phase (Fig. 3, Table 1). Spatial inhomogenities in the environments of individual molecules in polycrystalline films resulting in relaxation energy fluctuations have been considered as the major source of the broadening (33-37). Therefore the individual molecular bands due to intramolecular vibrations are no longer discernible in the photoemission spectrum of the solid. Furthermore, a temperature dependent phonon broadening has been considered (38). We note, that in addition to these processes a band bending $E(\underline{k})$ within the Brillouin zone will also contribute to a broadening of the valence bands. According to theoretical band structure calculations for other molecular crystals and experimental evidence for rare gas solids this $E(\underline{k})$ dispersion is expected to range between 0.3 eV and 1.5 eV (39).

3b Photoemission intensities, branching ratios and electronic band structure

Next we discuss the $h\nu$-dependence of the partial photoionization cross sections for the valence bands. Inspection of Fig. 2 shows immediately that the intensity of each of the primary peaks goes through a maximum at around 4.5 eV kinetic energy. The result of the detailed analysis is collected in Table 2 and displayed in Figs. 4 and 5. From the energy distribution curves, like those shown in Fig. 2, we obtain the relative partial ionization intensities $\sigma_i(h\nu)$ for the i-th band by measuring for each photon energy the area A_i under each peak. This procedure gives reliable results, because we are using an angle integrating analyzer and polycrystalline, randomly oriented samples, which can be regarded as an isotropic source of electrons. Therefore, all directions are averaged and no angular dependence should be observable.

Comparison of figures 4 and 5 shows that weaker structures show up at higher photon energies in the plot of branching

ratios (Fig. 5) which are not visible in the plot of ionization intensities (Fig. 4). Moreover, we would like to point out, that the branching ratios are quite similar to the gas phase results, whereas the partial cross sections are markedly different.

In order to discuss further the intensities and partial photoionization cross sections we briefly recall those factors which influence the intensity $I(E,\omega)$ of photoemitted electrons with energy E excited by photons of frequency ω from a solid sample (40). This will enable us also to make a comparison to the optical spectrum, more exactly to the imaginary part $\varepsilon_2(\omega)$ of the dielectric constant.

Within the framework of the three step model for photoemission (41) the intensity distribution of primary electrons $I(E,\omega)$ can be factorized:

$$I(E,\omega) = P(E,\omega) \times T(E) \times D(E)$$

according to the sequence of three events, namely (i) the optical excitation of an electron leading to a distribution of photoexcited electrons $P(E,\omega)$, (ii) the transport through the solid characterized by a transmission function T(E) and (iii) the escape through the sample surface into the vacuum described by the escape function D(E).

The transport function T(E) includes the possibility for inelastic scattering by the other electrons or elementary excitations in the solid. It is a slowly varying smooth function depending only on the energy E of the photoelectrons and reflecting the fact that no single scattering process characterized by one particular sharp threshold energy dominates electron transport. In molecular crystals such as solid CO_2, excitation of several electronic and vibrational excited states can contribute to the scattering of primary excited photoelectrons. The energies for such excitations range from a few meV for phonons and vibrational motions to several 100 meV for intramolecular vibrations and up to several eV for exciton excitation (see Fig. 7). Hence we do not expect to observe a sharp onset of a single dominating electron-scattering mechanism.

D(E), like T(E), is a smooth function of E beyond the threshold for which the energy of the electron E is sufficient to permit it to surmount the potential barrier at the surface. Because electron affinities are in the range of 1 eV for molecular crystals, the barrier is low and D(E) has negligible influence on the spectra. While both factors may distort the energy distribution they are not expected to introduce structure or peaks in the intensity distribution $I(E,\omega)$.

The spectrum of photoexcited electrons $P(E,\omega)$ is the remaining factor to be discussed. Within the three step model this distribution is given through the optical excitation of electrons from occupied valence band states E_v into empty conduction band states E_c:

$$P(E,\omega) \propto \sum_{v,c} \int d^3k \; |\underline{\underline{e}}\underline{\underline{M}}_{v,c}|^2 \delta(E_c - E_v - h\omega)\; \delta(E_c - E)$$

where $\underline{\underline{e}}\underline{\underline{M}}_{v,c}$ is the dipole matrix element for the optical transition. It should be noted that the photoemission in this model becomes a very selective process since three δ-functions (including the k-selection in the matrix element $|\underline{\underline{e}}\underline{\underline{M}}_{v,c}|$) restrict the possible contributions. The expression for $P(E,\omega)$ is closely related to $\varepsilon_2(\omega)$, the imaginary part of the dielectric constant (40):

$$\varepsilon_2(\omega) \propto \frac{1}{\omega^2} \sum_{v,c} \int d^3k \; |\underline{\underline{e}}\underline{\underline{M}}_{v,c}|^2 \; \delta(E_c - E_v - h\omega)$$

If we take the dipole matrix element to be constant $\varepsilon_2(\omega)$ is a measure for the joint density of states, that is the total number of transitions possible at a photon energy ω subject to energy and k-vector conservation. Likewise $P(E,\omega)$ gives the energy distribution of the joint density of states. Furthermore, if the valence bands are flat with no or little dispersion, then $\varepsilon_2(\omega)$ and $P(E,\omega)$ simply reflect the density of conduction band states.

3c Conduction Band Density of States

Molecular crystals have rather flat valence bands with only little dispersion, because the overlap of neighbouring molecules in a van der Waals-crystal is small. This is also the case for solid CO_2 where the width of the valence bands never exceeds 1.1 eV (see Figs. 2 and 3 and Table 1). If we further consider that this total width is an average over the intramolecular vibrational bands broadened by solid state effects (see section 3a), an upper limit of the $E(\underline{k})$ - dispersion in solid CO_2 is more likely 0.5-0.8 eV. Under these conditions the $h\nu$-dependent intensity variations in the EDC's reflect the conduction band density of states. We are thus lead to the conclusion that the maxima appearing for each partial ionization cross section are due to a high density of final conduction band states. The resulting schematic energy band scheme comprising valence and conduction bands is depicted in Fig. 6.

Our determination of the conduction band density of states from the direct photoemission is supported by the observation of pronounced maxima of scattered electrons in each EDC (Fig. 2) peaking at ~ 4.5 eV kinetic energy. These maxima are clearly visible for $h\nu \gtrsim 30$ eV where they are almost not obscured by primary emission. Their kinetic energy is independent of photon energy and thus they reflect the high density of final states in the conduction band into which primary electrons are scattered inelastically. This peak of scattered electrons grows with increasing photon energy since the number of successive scattering events, which one primary electron can undergo, increases with kinetic energy.

3d Shape resonances in solid CO_2

According to the discussion in the previous section one would clearly like to compare our data with band structure calculations, but in the absence of those calculations we first compare our data to gas phase results from x-ray absorption, valence shell

photoemission and electron scattering experiments in order to elucidate the molecular parentage of the observed resonances.

The photoionization cross sections of both valence shell and inner shell electrons as well as electron scattering cross sections are dominated by shape resonances. These resonances are quasibound continuum states in which an incoming or outgoing electron is trapped by a potential barrier. In small molecules the barrier is mainly a centrifugal one. Theoretically the resonance phenomena can be accounted for in the multiple scattering model or as virtual orbitals in molecular orbital calculations (see e.g. Ref. (42) and references therein). Since the shape resonances are localised in the inner part of the molecule the main difference between x-ray absorption, photoionization and electron scattering is a shift of the resonance energy to higher kinetic energy according to the different strength of Coulomb interaction encountered in each case and due to the different number of electrons involved (43). Therefore x-ray absorption spectra, electron scattering experiments and calculations can be used as a guide in deciding which shape resonances are to be expected in photoionization. For core shell ionization the interpretation is often facilitated compared to valence shell ionization, because only one or a few well localised initial orbitals are involved.

Returning now to the special case of CO_2, in electron scattering four shape resonances have been predicted (44,45) of which three are readily observed as shape resonances (46), namely in the π_u, σ_g and σ_u channel. In the core shell absorption spectra the π_u resonance where an electron occupies the $2\pi_u$ virtual orbital is observed as an intense peak in the discrete spectrum a few eV below the corresponding ionization threshold. From comparing theoretical calculations (15,16,18) and measured spectra (47-49) the σ_g and σ_u shape resonances are expected in the continuous spectrum, about 1 eV and 17 eV above threshold. We have collected the data concerning the resonances observed in x-ray absorption and electron scattering in Table 3. According

to dipole selection rules one can expect shape resonances to occur in photoemission from all four valence levels. Calculations (12,15-21) and measurements of gas phase cross sections and β parameters (8-14) largely agree with this expectation (see also Table 3).

Let us now briefly discuss the photoemission from the indiviual orbitals and the relevance of calculated and measured gasphase spectra to our solid state experiments.

$1\pi_g$ Orbital

According to dipole selection rules, photoemission from the $1\pi_g$ orbital can couple to the π_u and σ_u resonance. The π_u resonance is expected to form a prominent $1\pi_g \rightarrow 2\sigma_u$ valence transition around $h\nu$ = 12.5 eV (or 1.3 eV below the IP (7)), although the experimental identification is not unique. The $1\pi_g \rightarrow 4\sigma_u$ resonance is calculated at $h\nu$ = 20 eV (15,16) or $h\nu$ = 31-35 eV (12,17-21) however, when averaged over vibrational bands, the resonance is completely smeared out and not visible in experimental spectra (9-11,14). It is very interesting to note that our branching ratios for the $1\pi_g$ orbital show a clear maximum at $h\nu$ = 32 eV (E_{kin}=19 eV) which we consequently interprete as the $1\pi_g \rightarrow 4\sigma_u$ shape resonance (see Fig. 5). Obviously the crystal field leads to a modification of the molecular potential which brings out the resonance more clearly. Close to threshold the cross section is dominated by a maximum in the $1\pi_g \rightarrow \varepsilon\delta_u$ channel which is mostly of atomic origin ($2p \rightarrow \varepsilon d$) and contributes to the maximum we observe close to threshold.

$1\pi_u$ and $3\sigma_u$ Orbital

The $1\pi_u$ and $3\sigma_u$ orbital can only couple to the σ_g resonance which is calculated to be at $h\nu$ = 19-25 eV (15-18,20,21). One calculation (17,18) predicts even a minimum in the cross section. The cross section for the $1\pi_u$ orbital is again dominated by the atomic-like $1\pi_u \rightarrow \varepsilon\delta_g$ channel with a maximum close to threshold. For the $3\sigma_u$ and $1\pi_u$ orbitals the $3\sigma_u \rightarrow 5\sigma_g$ and $1\pi_u \rightarrow 5\sigma_g$ shape resonances are found immediately above threshold.

$4\sigma_g$ Orbital

Finally photoemission from the $4\sigma_g$ orbital can couple to the π_u and σ_u resonance. The $4\sigma_g \rightarrow 2\pi_u$ resonance is calculated (7,16) and experimentally assigned (7) below the threshold at $h\nu$ = 15.5 eV. The $4\sigma_g \rightarrow 4\sigma_u$ shape resonance is theoretically expected around $h\nu$ = 40 eV (12,17-21) (Ref. 15,16 gives $h\nu$ = 30 eV) and experimentally verified at $h\nu$ = 39-42 eV (13,14) in the asymmetry parameter . Partial cross sections in the gas phase show only a broad maximum at the resonance energy (9-11). Our measurements are restricted to photon energies below $h\nu$ = 40 eV, so that we cannot unambiguously identify a maximum in the $4\sigma_g$ branching ratio, which however seems to show a small rise in that region.

A synopsis of gas phase photoemission results in comparison with our data for solid CO_2 and an assignment of the final states appears in Table 4.

3e The Optical Spectrum of solid CO_2 in the VUV

According to Table 3, there is a "discrete" $2\pi_u$-shape resonance located ~ 6 eV below threshold. This resonance is expected to lead to a strong valence transition in the VUV absorption spectrum. Although the gas phase absorption spectrum (7,50) is rather complicated mainly because of overlapping Ryberg states, the $1\pi_g \rightarrow 2\pi_u$ transition has been assigned to an absorption band at $h\nu$ = 12.5 eV and the $4\sigma_g \rightarrow 2\sigma_u$ transition to a band at $h\nu$ = 15.5 eV (7).

Together with our photoemission results we can now reach an interpretation of the hitherto unassigned solid state $\varepsilon_2(\omega)$-spectrum (23). The imaginary part of the dielectric function (Fig. 7) shows in the VUV a fairly simple irregular structure

with sharp intense maxima at around 10.4 eV, 12.8 eV and 14.6 eV and a broader structured region with its maximum roughly at 20.8 eV (see Fig. 7). As discussed in section 3b and 3c we can obtain the density of valence to conduction band transitions by adding up the partial photoemission cross sections (Fig. 7). We are thus lead to a simple interpretation of the optical spectrum. All structure appearing at photon energies $h\nu < 13$ eV has to be attributed to exciton states. The maximum at ~ 15 eV may be due to a metastable exciton state. The broad optical band centered at 20,8 eV is then due to interband transitions.

In solid N_2 and CO the excitons are of the Frenkel type and have a definite parentage in electronic excitations of a single molecule, constituting stable crystal excitations below the interband transition to the conduction band (51). Similarily for solid CO_2 we can assume that the stable exciton states below the onset of interband transitions at 13 eV have their origin in electronic states in the 10-15 eV range of the gas phase spectrum (7,52).

An inspection of the excitation spectrum of CO_2 (52) and the schematic energy scheme in Fig. 6 strongly suggests that the strong dominating gas phase bands at 11.05 and 11.38 eV, the so called "main-band" and "minor-band", give rise to the strong exciton band at 10.6 eV in the solid, labeled I in Figs. 6 and 7. These intense broad bands in the gas phase have previously en described as the lowest $n = 3$ members of $1\pi_g \rightarrow np\sigma_u$ and $1\pi_g \rightarrow np\sigma_u$ Rydberg series (7). Since Rydberg states, because of their large spatial extend are strongly quenched and are generally not observed in the solid (53), we have to postulate either valence character for the "main"- and "minor-band" or a strong admixture of valence character to these bands in the gas phase.

The two maxima II and III are located at $h\nu = 12$-14 eV and $h\nu = 14$-16 eV (Fig. 7). The gas phase spectrum shows many Rydberg states in this energy range which are again expected to be strongly quenched in the solid. However, as discussed above the two "discrete" shape resonances fall in this energy range.

We therefore suggest to assign the maximum II as the $1\pi_g \rightarrow 2\pi_u$ ($\pi \rightarrow \pi^*$) and the maximum III as the $4\sigma_g \rightarrow 2\pi_u$ ($\sigma \rightarrow \pi^*$) transition. Exciton II is located at threshold. It therefore has to be regarded as a metastable exciton or a shape resonance respectively.

3f Solid state effects in the bandstructure of solid CO_2

So far we have discussed the photoemission results for solid CO_2 in close analogy to gas phase data and found a close one to one correspondence in the initial states. In the preceeding section we could even propose new assignments for the excitons ("discrete" shape resonances) in solid CO_2 based on a comparison of gas-phase and solid-phase absorption data. In view of this close analogy it seems interesting and important to further compare results from other kinds of experiments and to explore the nature of the shape resonances more completely.

In Fig. 8 we have plotted the observed excitation energies of shape resonances in x-ray absorption, gas-phase and solid-phase photoemission and electron scattering on a common energy scale. A clear trend towards higher kinetic energies is observed for each resonance in going from x-ray absorption to electron scattering. This increase in excitation energy reflects the increasing Coulombic repulsion of the electron. Fig. 8 also shows that the 4.5 eV resonance observed for solid CO_2 in photoemission is close to the e^--scattering resonance which has $2\pi_u$-character (46). The question still remains of what is the microscopic origin for this high density of conduction band states in solid CO_2. Certainly the $5\sigma_g$ shape resonance will contribute, as do the atomic $p \rightarrow \varepsilon d$ components, but the comparatively weak intensities for these channels in the gas-phase photoemission show that this cannot be the major contribution. Based on the similarity in energy between the $2\pi_u$-resonance in e^--scattering and the observed high conduction band density of states at about the same energy we suggest an intermolecular charge transfer mechanism as the major contribution whereby an excited electron

leaves the molecule and occupies the $2\pi_u$-scattering resonances of the neighbouring neutral molecules. In solid state language the scattering resonances form the conduction band states and the observed cross section maxima are real band-structure effects and can no more be considered as localized molecular excitations. We point out that this mechanism is likely to be the origin for similar observations for solid N_2 (1), where completely analogous arguments are valid.

Acknowledgement

We have profited from stimulating discussions with V. Saile and T.O. Woodruff during the experiments and while the manuscript was prepared. We would also like to acknowledge the continuous and efficient support of the technical staff of HASYLAB.

References

1 H.-J. Lau, J.-H. Fock and E.E. Koch, Chem. Phys. Lett. 89, 281 (1982)

2 D.W. Turner, C. Baker, A.D. Baker and C.R. Brundle, "Molecular Photoelectron Spectroscopy", Wiley-Interscience, New York, 1970

3 K. Kimura, S. Katsumata, Y. Achiba, T. Yamazaki and S. Iwata, "Handbook of HeI Photoelectron Spectra of Fundamental Organic Molecules", Japan Scientific Societies Press, Tokyo, 1981

4 A.W. Potts and T.A. Williams, J. Elec. Spec.3, 3 (1974)

5 L.S. Cederbaum, J. Schirmer, W. Domcke and W. von Niessen, J. Phys. B 10, L549 (1977)

6 B. Kellerer, L.S. Cederbaum and G. Hohlneicher, J. Elec. Spec. 3, 107 (1974)

7 G. Eridh, L. Åsbrink and E. Lindholm, Chem. Phys. 27, 169 (1978)

8 L.C. Lee, R.W. Carlson and D.L. Judge, J. Phys. B 9, 855 (1976)

9 T. Gustafsson, E.W. Plummer, D.E. Eastman and W. Gudat, Phys. Rev. A 17, 175 (1978)

10 C.E. Brion and K.H. Tan, Chem. Phys. 34, 141 (1978)

11 C.E. Brion and K.H. Tan, J. Elec. Spec. 15, 241 (1979)

12 F.A. Grimm, T.A. Carlson, W.B. Dress, P. Agron, J.O. Thomson and J.W. Davenport, J. Chem. Phys. 72, 3041 (1980)

13 T.A. Carlson, M.O. Krause, F.A. Grimm, J.D. Allen Jr., D. Mehaffy, P.R. Keller and J.W. Taylor, Phys. Rev. A 23, 3316 (1981)

14 F.A. Grimm, J.D. Allen Jr., T.A. Carlson, M.O. Krause, D. Mehaffy, P.R. Keller and J.W. Taylor, J. Chem. Phys. 75, 92 (1981)

15 P.W. Langhoff, N. Padial, G. Csanak, T.N. Rescigno and B.V. McKoy, J. Chim. Phys. (Paris) 77, 589 (1980)

16 N. Padial, G. Csanak, B.V. McKoy and P.W. Langhoff, Phys. Rev. A 23, 218 (1981)

17 R.R. Lucchese and V. McKoy, J. Phys. Chem. 85, 2166 (1981)

18 R.R. Lucchese and V. McKoy, Phys. Rev. A 26, 1406 (1982)

19 J.R. Swanson, D. Dill and J.L. Dehmer, J. Phys. B 13, L231 (1980)

20 J.R. Swanson, D. Dill and J. L. Dehmer, J. Phys. B 14, L207 (1981)

21 F.A. Grimm, J.D. Allen Jr., T.A. Carlson, M.O. Krause, D. Mehaffy, P.R. Keller and J.W. Taylor, J. Chem. Phys. 75, 92 (1981)

22 M.J. Campbell, J. Liesegang, J.D. Riley and J.G. Jenkin, J. Phys. C 15, 2549 (1982)

23 E.E. Koch and M. Skibowski, Chem. Phys. Lett. 14, 37 (1972)

24 V. Saile, P. Gürtler, E.E. Koch, A. Kozevnikov, M. Skibowski and W. Steinmann, Appl. Optics 15, 2559 (1976)

25 P.W. Palmberg, J. Elec. Spec. 5, 691 (1974)

26 P.W. Palmberg, J. Vac. Sci. Technol. 12, 379 (1975)

27 R.W.G. Wyckoff, "Crystal Structures", Vol. 1, Wiley-Interscience, New York, 1965

28 P.S. Bagus and K. Hermann, Solid State Comm. 20, 5 (1976)

29 K. Hermann and P.S. Bagus, Phys. Rev. B 16, 4195 (1977)

30 N.F. Mott, M.J. Littleton, Trans. Faraday Soc. 34, 485 (1938)

31 F. Gutman and E. Lyons, "Organic Seminconductors", John Wiley, New York, 1967

32 F.-J. Himpsel, N. Schwentner and E.E. Koch, phys. stat. sol. (b) 71, 615 (1975)

33 C.B. Duke, W.R. Salaneck, T.J. Fabish, J.J. Ritsko, H.R. Thomas and A. Paton, Phys. Rev. B. 18, 5717 (1978)

34 C.B. Duke, in: J.S. Miller, Ed., "Extended Linear Chain Compounds", Vol. 2, Plenum Press, New York, 1982, p. 59

35 W.R. Salaneck, in: D.W. Dwight, T.J. Fabish and H.R. Thomas, Eds., "Photon, Electron and Ion Probes of Polymer Structure and Properties", American Chemical Society Symposium Series 162, Washington D.C., 1981, p. 121

36 C.B. Duke, T.J. Fabish and A. Paton, Chem. Phys. Lett. 49, 133 (1977)

37 W.R. Salaneck, Phys. Rev. Lett. 40, 60 (1978)

38 W.R. Salaneck, C.B. Duke, W. Eberhardt, E.W. Plummer and H.J. Freund, Phys. Rev. Lett. 45, 280 (1980)

39 N. Schwentner, F.-J. Himpsel, V. Saile, M. Skibowski, W. Steinmann and E.E. Koch, Phys. Rev. Lett 34, 528 (1975)

40 See e.g. M. Cardona and L. Ley in: "Photoemission in Solids", Vol. 1, M. Cardona and L. Ley, Eds., Topics in Applied Physics Vol. 26, Springer Verlag, Berlin, Heidelberg, New York, 1978, p. 84

41 See e.g. C.N. Berglund and W.E. Spicer, Phys. Rev. 136, A 1030 (1964)

42 M.J. van der Wiel in: "Electronic and Atomic Collisions", N. Oda and K. Takayanagi, Eds., North Holland Publ. Company, Amsterdam, 1980, p. 209

43 J.L. Dehmer and D. Dill, in: "Symp. on Electron-Molecule Collisions", I. Shimamura and H. Matsuzawa, Eds., University of Tokyo, 1974, p. 95

44 D. Dill, J. Welch, J.L. Dehmer and J. Siegel, Phys. Rev. Lett 43, 1236 (1979)

45 M.G. Lynch, D. Dill, J. Siegel and J.L. Dehmer, J. Chem. Phys. 71, 4249 (1979)

46 M. Tronc, R. Azria and R. Paineau, J. Phys. (Paris) 40, L323 (1979)

47 G.R. Wight and C.E. Brion, J. Elec. Spec. 3, 191 (1974)

48 M. Tronc, G.C. King and F.H. Read, J. Pyhs. B 12, 137 (1979)

49 D.M. Barrus, R.L. Blake, A.J. Burek, K.C. Chambers and A.L. Pregenzer, Phys. Rev. A 20, 1045 (1979)

50 L.C. Lee, R.W. Carlson, D.L. Judge and M. Ogawa, J. Quant. Spectrosc. Radiat. Transfer, 13, 1023 (1973)

51 For a recent discussion see: J. Jortner, E.E. Koch and N. Schwentner, in: "Photophysics and Photochemistry in the Vacuum Ultraviolet", S. McGlynn, G. Findley and R. Huebner, Eds., D. Reidel Publ. Company, Dordrecht, Holland, 1983

52 E.N. Lassettre, A. Skerbele, M.A. Dillon and K.J. Ross, J. Chem. Phys. 48, 5066 (1968) and M. Krauss, S.R. Mielczarek, D. Neumann and C.E. Kuyatt, J. Geophys. Res. 76, 3733 (1971)

53 M.B. Robin, Higher Excited States of Polyatomic Molecules, Vol. I, Academic Press, New York, London, 1974

Initial Orbital	Solid (this work) IP_{vert} (eV)	FWHM (eV)	IP_{ad} (eV)	Gas Ref.(2) IP_{vert} (eV)	IP_{ad} (eV)	Shift ΔIP_{vert} (eV)	ΔIP_{ad} (eV)
$1\pi_g$	13,0	0,95	11,9	13,78	13,78	0,8	1,9
$1\pi_u$	16,7	1,10	15,4	17,59	17,32	0,9	1,9
$3\sigma_u$	17,6	0,85	16,6	18,08	18,08	0,5	1,5
$4\sigma_g$	18,8	0,80	17,8	19,4	19,4	0,6	1,6

Table 1: Vertical (IP_{vert}) and adiabatic (IP_{ad}) ionization potentials, full width half maximum (FWHM) and energy shift between gas and solid. For the solid phase the adiabatic ionization potential has been determined according to the formula $IP_{ad} = IP_{vert} - (1,2 \times FWHM)$.

hν (eV)	relative cross section weighting factor	$1\pi_g$	$1\pi_u+3\sigma_u$	$4\sigma_g$	branching ratio $1\pi_g$	$1\pi_u+3\sigma_u$	$4\sigma_g$
16	1	1.204			1		
17	1	2.070			1		
17.5	1	2.311			1		
18	1	2.653			1		
18.5	1	2.593			1		
19	1	2.099	0.311		0.87	0.13	
19.5	1	1.856	0.670		0.73	0.26	
20	1	1.549	1.365		0.53	0.47	
20.5	1	1.274	2.130		0.37	0.63	
21	1	1.068	2.952	0.110	0.26	0.71	0.03
22	1	0.721	3.056	0.310	0.18	0.75	0.07
23	1	0.434	2.154	0.442	0.14	0.71	0.15
24	1	0.272	1.274	0.244	0.15	0.71	0.14
25	1	0.180	0.862	0.269	0.14	0.66	0.20
25	6.8	1.422	5.708	1.561	0.16	0.66	0.18
26	6.8	1.031	3.518	1.083	0.18	0.63	0.19
27	6.8	0.731	2.088	0.554	0.22	0.62	0.16
28	6.8	0.530	1.195	0.321	0.26	0.58	0.16
29	6.8	0.418	0.887	0.276	0.26	0.56	0.17
30	6.8	0.414	0.671	0.184	0.33	0.53	0.14
31	6.8	0.393	0.588	0.143	0.35	0.52	0.13
32	6.8	0.468	0.603	0.166	0.38	0.49	0.13
33	6.8	0.511	0.667	0.207	0.37	0.48	0.15
34	6.8	0.447	0.631	0.204	0.35	0.50	0.16
35	6.8	0.433	0.639	0.227	0.33	0.49	0.17
36	6.8	0.332	0.551	0.199	0.31	0.51	0.18
37	6.8	0.276	0.470	0.198	0.29	0.50	0.21
38	6.8	0.185	0.325	0.126	0.29	0.51	0.20
39	6.8	0.149	0.273	0.100	0.28	0.52	0.19
40	6.8	0.141	0.255	0.093	0.29	0.52	0.19

Table 2 Relative cross section data and branching ratios plotted in figures 4 and 5. The weighting factor is due to different pass energies of the electron analyzer.

final Orbital	E_{kin} (eV) A	B	ΔE_{kin} (eV) A - B
$2\tau_u$	-6,8 (C1s)	3,8	-10,6
	-5,7 (O1s)		- 9,5
$5\sigma_g$	0,8 (O1s)	10,8	-10,0
$4\sigma_u$	16,5 (C1s)	30,0	-13,5
	17,6 (O1s)		-12,4

Table 3: Shape resonances for CO_2 observed in X-ray absorption A (47-49) and electron scattering B (46). The minus sign in X-ray absorption indicates that the resonances occur in the discrete part of the spectrum below threshold.

initial Orbital	Solid this work hν (eV)	E_{kin}(eV)	Gas (see text) hν (eV)	E_{kin}(eV)	assignment
$1\pi_g$	12-14	(-1)-(+1)	12,5	-1,28	$1\pi_g \rightarrow 2\pi_u$
	18,2	5,2	-	-	conduction band
	32,0	19,0	(31-35)	(16-20)	$1\pi_g \rightarrow 4\sigma_u$
$1\pi_u+3\sigma_u$	-	-	21,0	3,4	$1\pi_u \rightarrow 5\sigma_g$
	-	-	21,0	2,9	$3\sigma_u \rightarrow 5\sigma_g$
	22,0	4,4-5,3	-	-	conduction band
$4\sigma_g$	14-16	-(2,8-4,8)	15,5	-3,9	$4\sigma_g \rightarrow 2\pi_u$
	21,0	4,2	-	-	conduction band
	-	-	39-42	20-23	$4\sigma_g \rightarrow 4\sigma_u$

Table 4: Observed features in photoemission cross sections and VUV absorption for gaseous and solid CO_2. The minus sign for kinetic energies indicated that the features occur in the discrete part of the spectrum below threshold. These values are taken from absorption data (see text).

Figure Captions

Fig. 1 Experimental set up for the study of photoelectron emission from condensed gases deposited at low temperatures (T = 7-300 K).

Fig. 2 Photoelectron energy distribution curves for polycrystalline solid CO_2 for excitation energies ranging between 14 and 40 eV. In this plot the same initial states follow inclined lines. The four valence molecular orbitals are denoted by the one-electron MO-notation.

Fig. 3 Comparison of the gas phase photoelectron spectrum from Turner et al. (2) (upper panel) with a photoelectron energy distribution curve for solid CO_2 (this work, lower panel). ΔE_R^v = 0.7 eV gives the rigid gas-to-soild relaxation shift by which the gas phase spectrum has been shifted in order to obtain coincidence for the prominent features. The deconvolution of the EDC for solid CO_2 into four bands is also shown. Crosses give the measured EDC while the solid line gives the sum of the indiviual bands (dashed curves).

Fig. 4 Relative partial ionization cross sections for the $1\pi_g$-derived, $1\pi_u + 3\sigma_u$-derived and $4\sigma_g$-derived valence bands of solid CO_2. The arrows mark the onset for photoemission from these bands.

Fig. 5 Branching ratios for the one electron states of CO_2. Note in particular the maximum in the $1\pi_g$ channel at hν = 32 eV corresponding to E_{kin} = 19 eV.

Fig. 6 Schematic energy scheme for the electronic band structure of solid CO_2 (right part). In order to deduce the molecular parentage comparison is made to the valence MO's and some excited states in gaseous CO_2 (see text).

Fig. 7 Comparison of the optical VUV-spectrum (dielectric function ε_2) of solid CO_2 (23) with the partial and summed photoionization cross sections as determined in this work. The excitonic nature of features I, II and III in the optical spectrum is clearly visible.

Fig. 8 Plot of shape resonances observed for CO_2 in x-ray absorption, gas phase and solid-phase ultraviolet photoelectron spectroscopy and in electron-scattering. Negative kinetic energies denote "discrete" shape resonances below threshold.

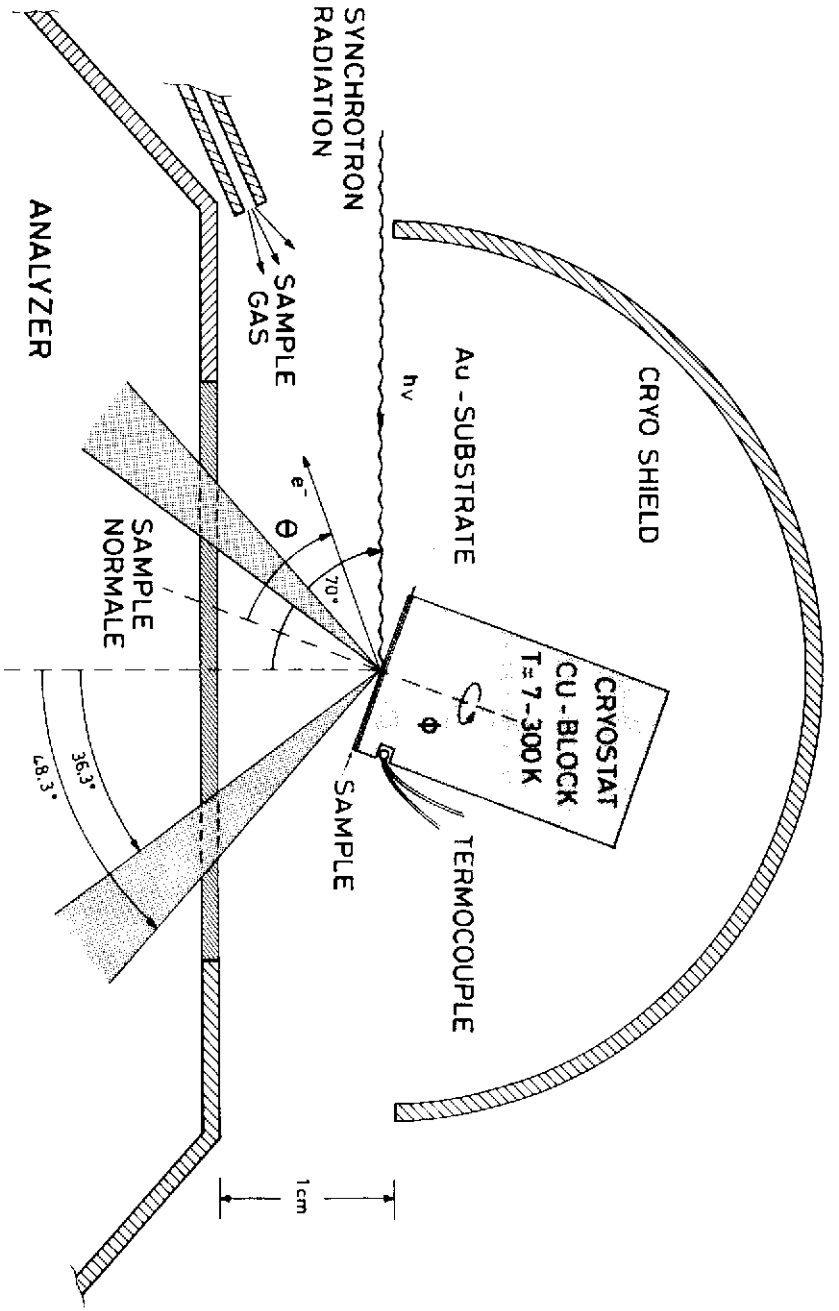

Fig. 1

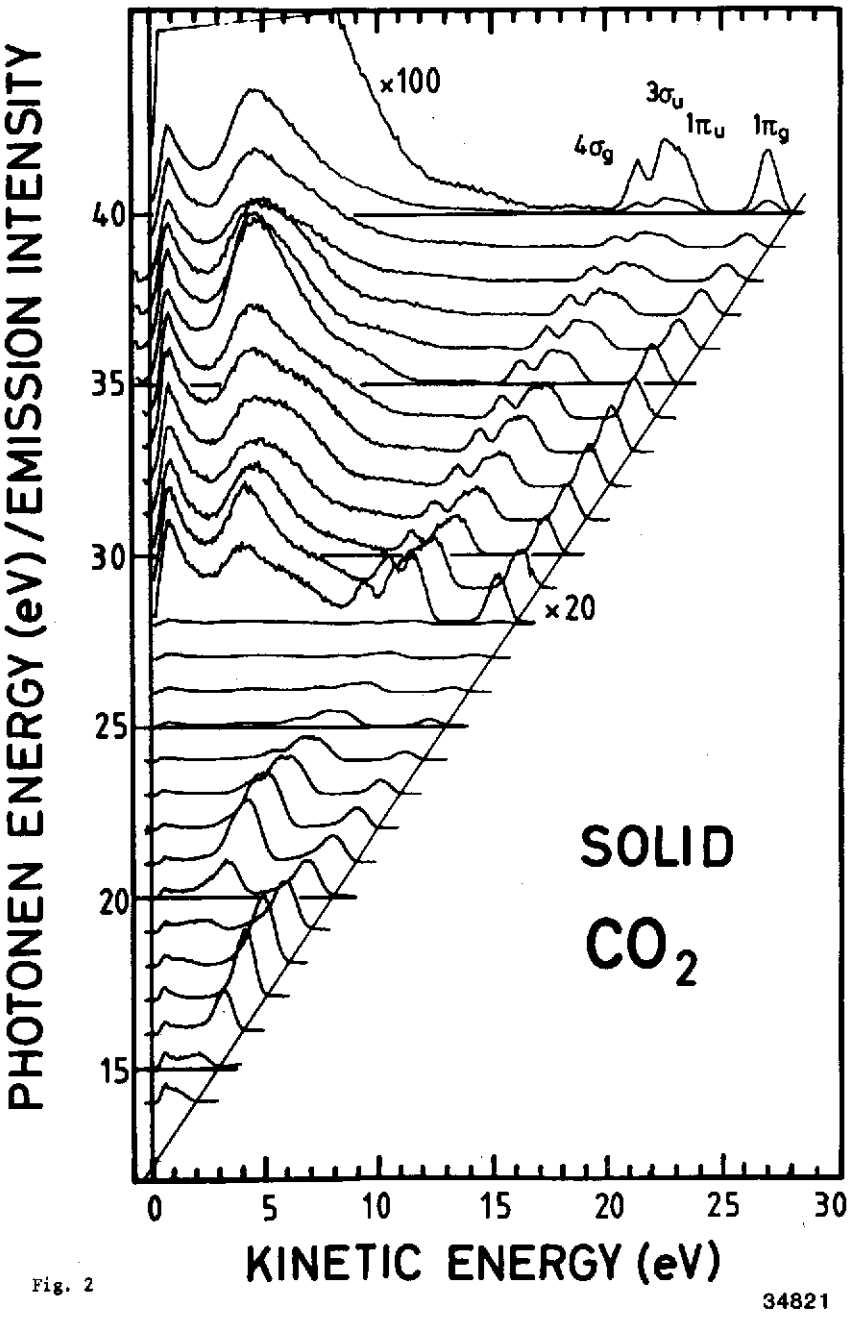
PHOTONEN ENERGY (eV)/EMISSION INTENSITY
KINETIC ENERGY (eV)
SOLID
CO_2
×100
×20
$4\sigma_g$
$3\sigma_u$
$1\pi_u$
$1\pi_g$
40
35
30
25
20
15
0
5
10
15
20
25
30
34821

Fig. 2

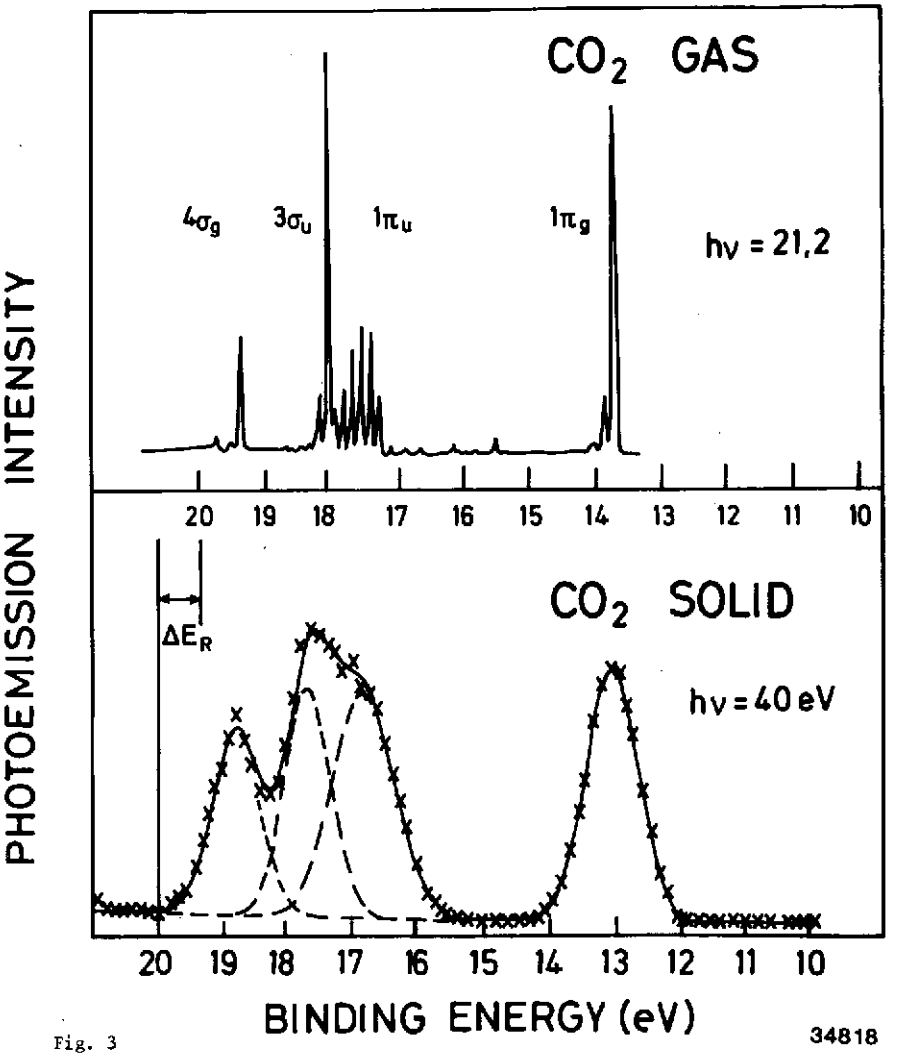
PHOTOEMISSION INTENSITY
CO_2 GAS
$4\sigma_g$
$3\sigma_u$
$1\pi_u$
$1\pi_g$
hν = 21,2
20 19 18 17 16 15 14 13 12 11 10
CO_2 SOLID
ΔE_R
hν = 40 eV
20 19 18 17 16 15 14 13 12 11 10
BINDING ENERGY (eV)
34818

Fig. 3

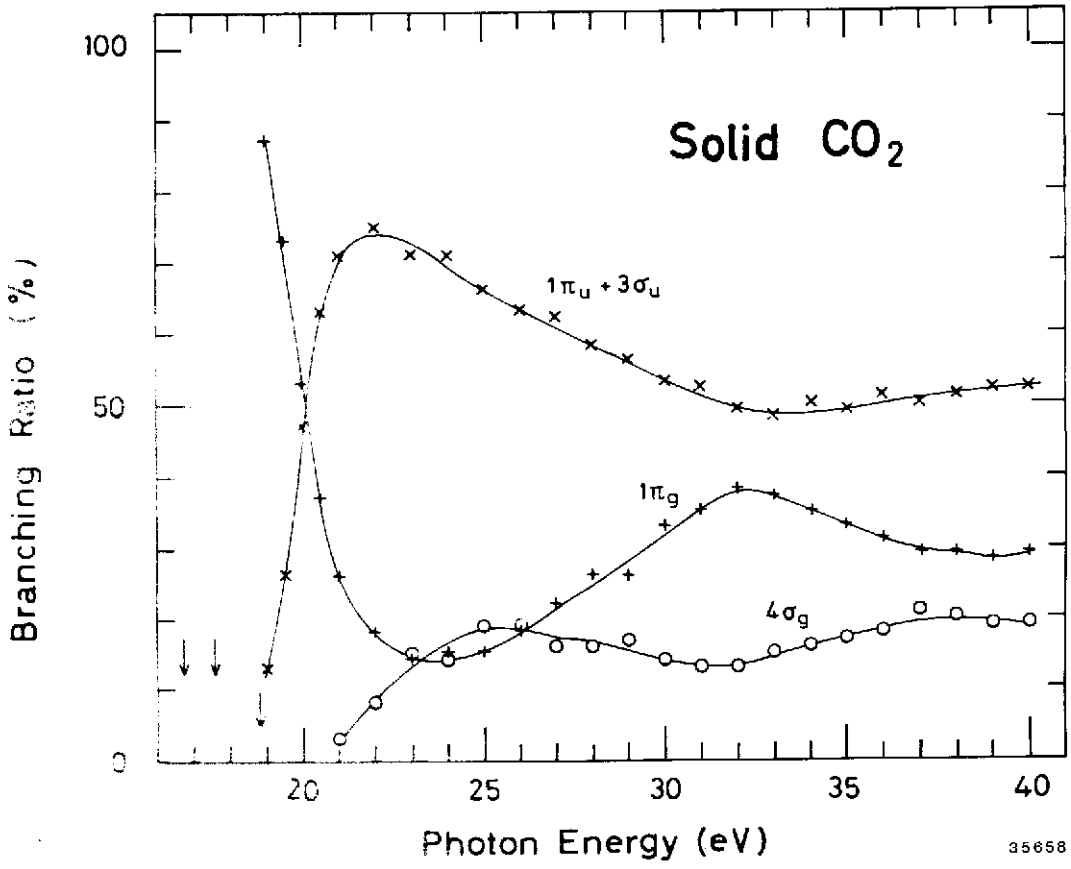
Solid CO_2
Branching Ratio (%)
100
50
0
20
25
30
35
40
Photon Energy (eV)
$1\pi_u + 3\sigma_u$
$1\pi_g$
$4\sigma_g$
35658

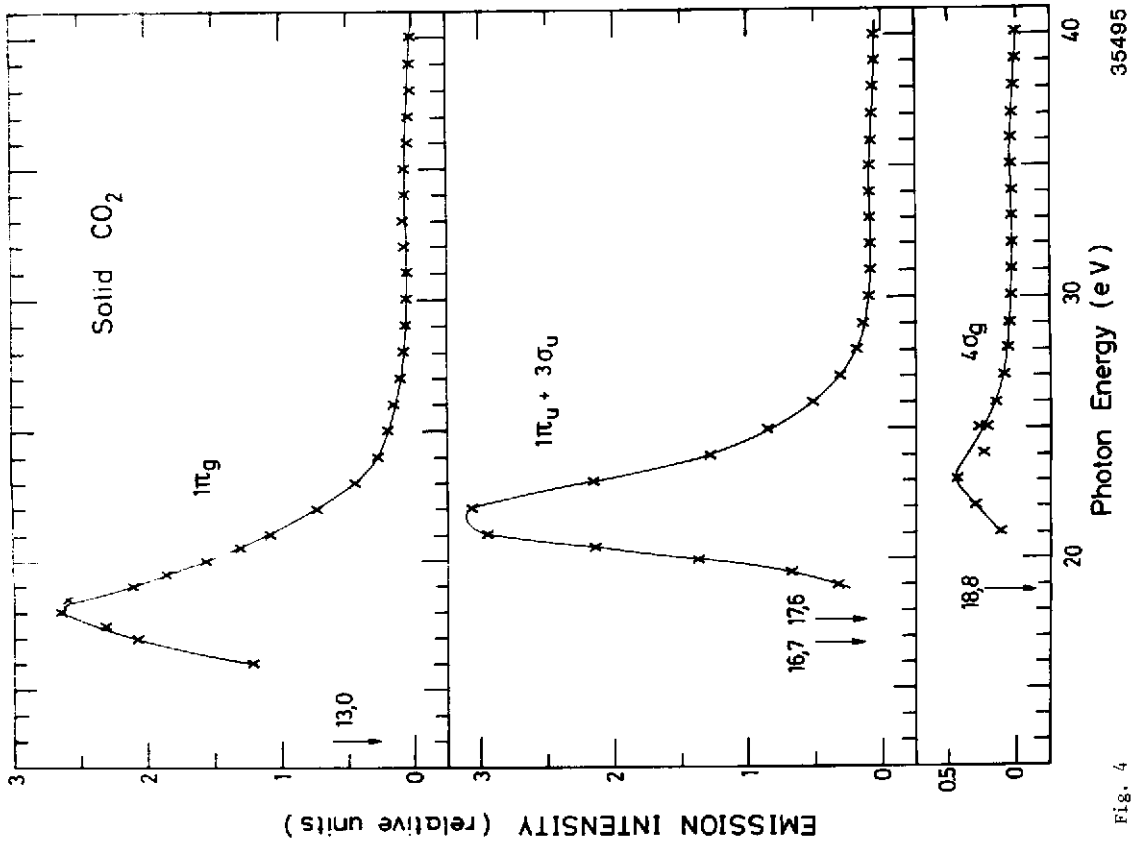
Solid CO_2
$1\pi_g$
13,0
$1\pi_u + 3\sigma_u$
16,7
17,6
$4\sigma_g$
18,8
EMISSION INTENSITY (relative units)
Photon Energy (eV)
35495

Fig. 4

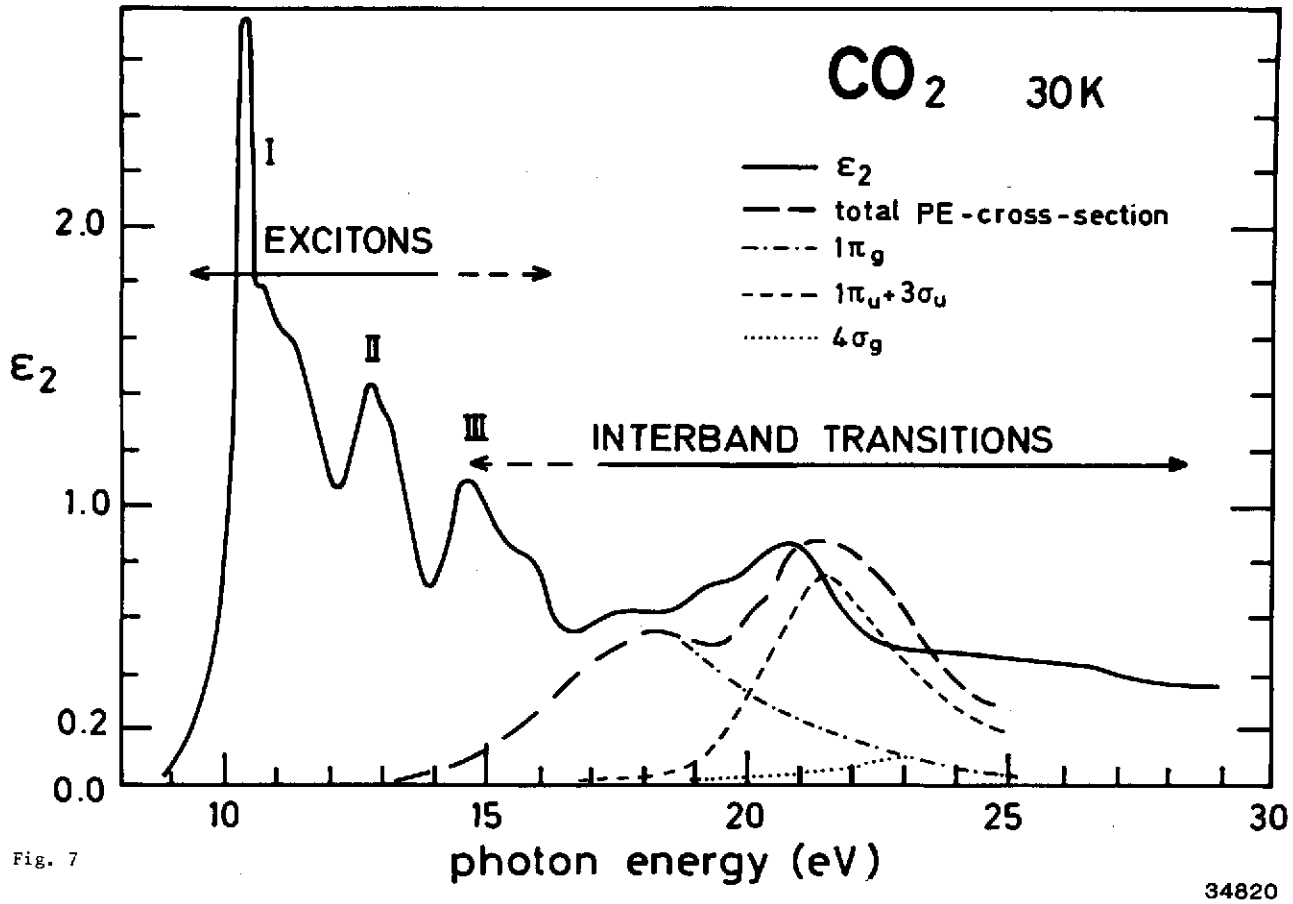
CO2 30K
ε2
total PE-cross-section
1πg
1πu+3σu
4σg
I
II
III
EXCITONS
INTERBAND TRANSITIONS
ε2
2.0
1.0
0.2
0.0
10
15
20
25
30
photon energy (eV)
34820

Fig. 7

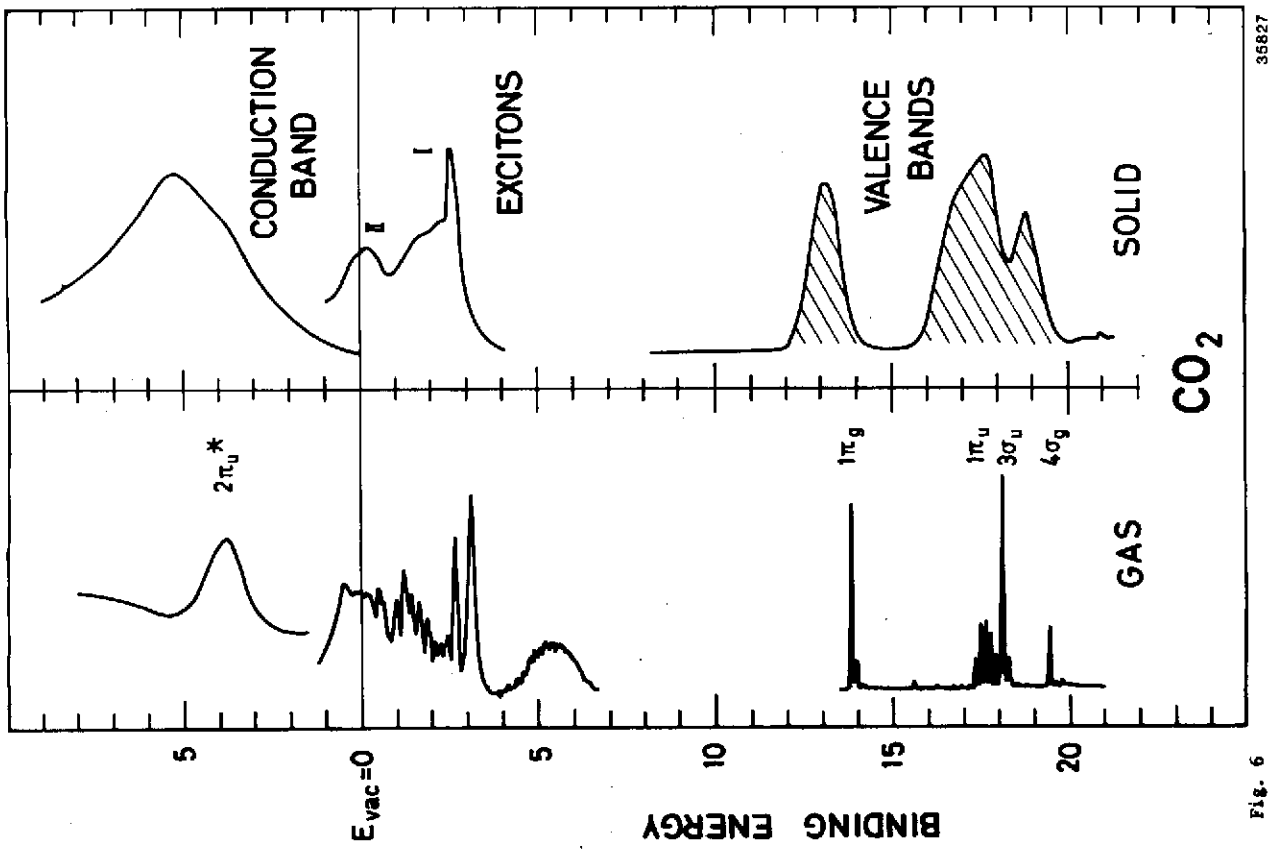
CONDUCTION BAND
EXCITONS
I
II
VALENCE BANDS
SOLID
CO2
2πu*
1πg
1πu
3σu
4σg
GAS
5
Evac=0
5
10
15
20
BINDING ENERGY
35827

Fig. 6

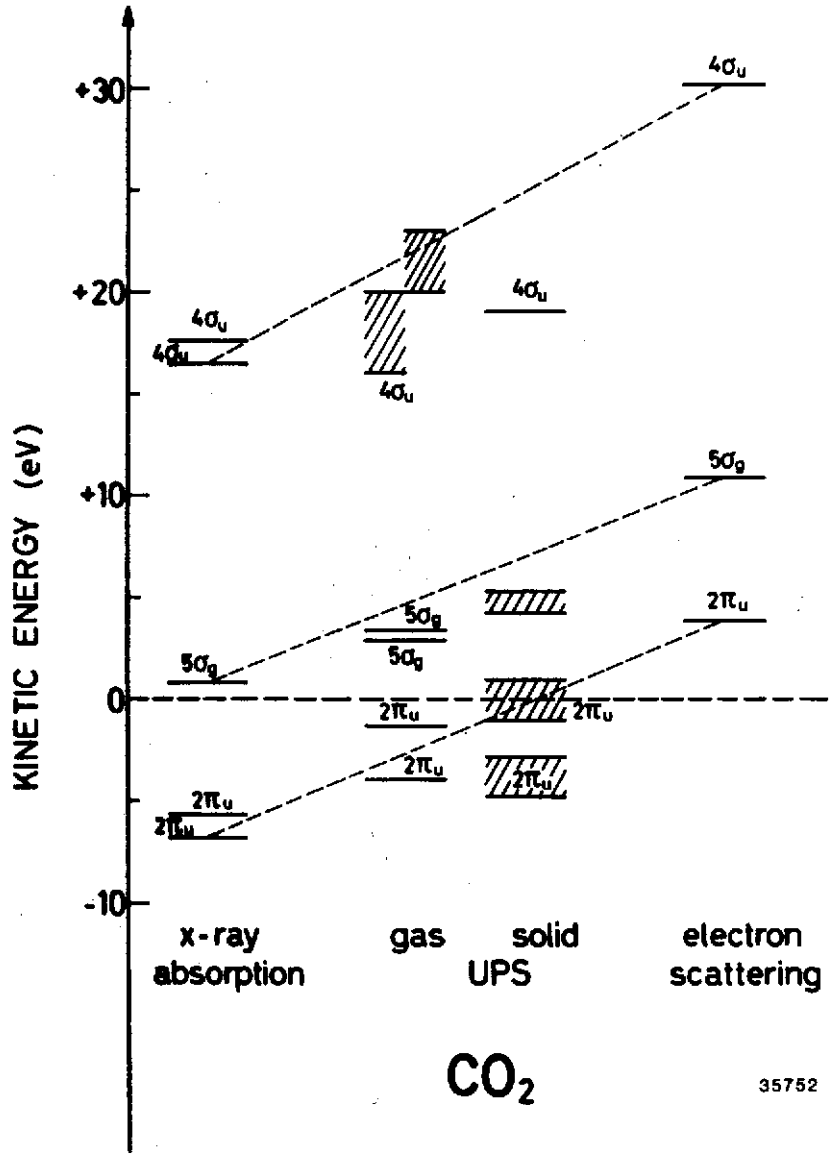
KINETIC ENERGY (eV)
+30
+20
+10
0
-10
4σu
4σu
4σu
4σu
4σu
5σg
5σg
5σg
2πu
2πu
2πu
2πu
2πu
2πu
x-ray absorption
gas
solid
UPS
electron scattering
CO2
35752

Fig. 8